

Emergence of quasiperiodic behavior in transport and hybridization properties of clean lattice systems

Cecilie Glittum , Antonio Štrkalj , and Claudio Castelnovo 

TCM Group, Cavendish Laboratory, J. J. Thomson Avenue, Cambridge CB3 0HE, United Kingdom

 (Received 13 October 2022; revised 29 November 2022; accepted 6 December 2022; published 6 February 2023)

Quasiperiodic behavior is mostly known to occur in systems with enforced quasiperiodicity or randomness, in either the lattice structure or the potential, as well as in periodically driven systems. Here, we present instead a rarer setting where quasiperiodic behavior emerges in clean, nondriven lattice systems. We illustrate this through two examples of experimental relevance, namely an infinite tight-binding chain with a gated segment, and a hopping particle coupled to static Ising degrees of freedom. We show how the quasiperiodic behavior manifests in the number of states that are localized by the geometry of the system, with corresponding effects on transport and hybridization properties.

DOI: [10.1103/PhysRevResearch.5.013083](https://doi.org/10.1103/PhysRevResearch.5.013083)

I. INTRODUCTION

Some of the most striking discoveries in physics occur when simple systems are found to exhibit unexpectedly complex behavior. These are often prime examples of the beauty and elegance of mathematical modeling that succeeds in describing the world around us. Examples include the chaotic motion of the double pendulum [1,2] and the quantum Hall effect of a 2D electron gas in a strong applied field [3].

Without claim of drawing a comparison in importance, we present here a simple result that fits well in this category. In one of its simplest forms, our finding shows that the number of states localized [4] on a gated portion of an infinite tight-binding chain forms a *quasiperiodic* sequence in the number of gated sites. Equivalently, the number of resonance peaks in the conduction along the chain also forms a quasiperiodic sequence. This happens for both negative and positive gate potential, within the bounds of the tight-binding band. We provide both an exact solution to the problem as well as a simple, elegant, and intuitive (albeit only effective) derivation of the same solution.

Our results are of direct relevance to several experimental settings—thinking for example about cold atoms [5,6], trapped ions [7,8], quantum dot arrays [9], superconducting qubits [10], and other quantum simulators [11]—and can be readily verified in a laboratory. Moreover, in addition to this simplest formulation of the problem, we show that a similar phenomenology is expected to play a role in other settings, for instance when particles hopping on a lattice are coupled to underlying spin degrees of freedom, as in the Falicov-Kimball

model [12] and in systems that exhibit disorder-free localization [13].

Quasiperiodic systems have received significant attention of late (see for instance Refs. [14–28]). In most cases however the quasiperiodicity is built into the system, e.g., via quasiperiodic modulation of on-site potentials and hopping amplitudes, or induced by incommensurate periodic driving; then, properties deriving from it are studied. Examples where quasiperiodicity is not seeded but rather emerges from periodic constituents are rare (most notably this was uncovered to result from the interplay of lattice filling fractions and interactions in Refs. [29,30]; however, see also Ref. [31] for an example of a quasicrystalline potential emerging from collective light scattering). In our setting, the quasiperiodic behavior emerges in a clean system made of nondriven periodic components—something that does not happen often in nature. We envision that the simple mechanism discussed in this work is likely to operate in interesting ways in other condensed matter systems, and possibly in higher dimensions as well.

II. GATED CHAIN

We study a tight-binding chain of lattice spacing $a = 1$ and hopping amplitude $t = 1$, with a segment of length L gated at potential, i.e., on-site energy, V_0 . The rest of the system (i.e., the left and right leads) is kept at the reference potential $V = 0$. The Hamiltonian of the system is given by

$$H = -t \sum_i [c_{i+1}^\dagger c_i + \text{H.c.}] + \sum_i V_i c_i^\dagger c_i, \quad (1)$$

where V_i is finite on the gated segment and vanishes on the leads. The system is illustrated in Fig. 1(a).

Due to the mismatch in on-site potential between the gated segment and the leads, some states localize on the gated segment, while other states are extended over the whole system. Our goal is to investigate the nature of these localized states, and more precisely how their number changes with the system parameters L and V_0 . As we detail below, the number of

Published by the American Physical Society under the terms of the [Creative Commons Attribution 4.0 International license](https://creativecommons.org/licenses/by/4.0/). Further distribution of this work must maintain attribution to the author(s) and the published article's title, journal citation, and DOI.

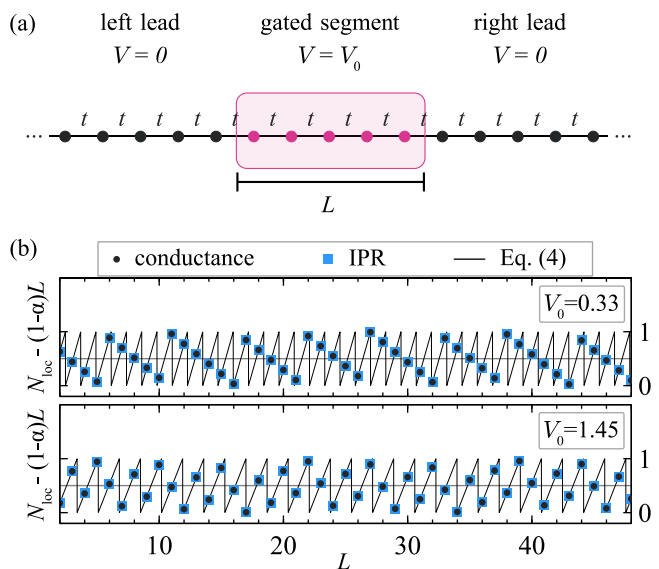


FIG. 1. (a) Illustration of the gated chain. The solid black dots illustrate the infinite leads, at potential $V = 0$. The solid pink dots illustrate the gated segment of length L at potential V_0 , here for $L = 5$. (b) Number of states localized in the gated region N_{loc} as a function of its length L . We subtracted the linear slope $(1 - \alpha)L$ to emphasize the quasiperiodic nature of the fluctuations following from sampling at integer L . Numerically obtained data from conductance simulations (black dots) and IPR (blue squares) overlap and agree perfectly with the analytical prediction in Eq. (4) (black line).

states Wannier-Stark-localized on the gated segment forms a *quasiperiodic* sequence as a function of the discrete length L of the segment; see Fig. 1(b).

By choosing an appropriate ansatz for the wave function, we look for eigenstates of the Schrödinger equation that are exponentially decaying on the leads (i.e., localized on the gated segment); see Appendix A for details and Appendix F for examples of wave function profiles. We find that the number of such states corresponds to the number of solutions of either of the following equations:

$$-e^{\text{arccosh}[V_0/2 - \cos k]} = \frac{\cos[k - k\frac{L+1}{2}]}{\cos[-k\frac{L+1}{2}]}, \quad (2)$$

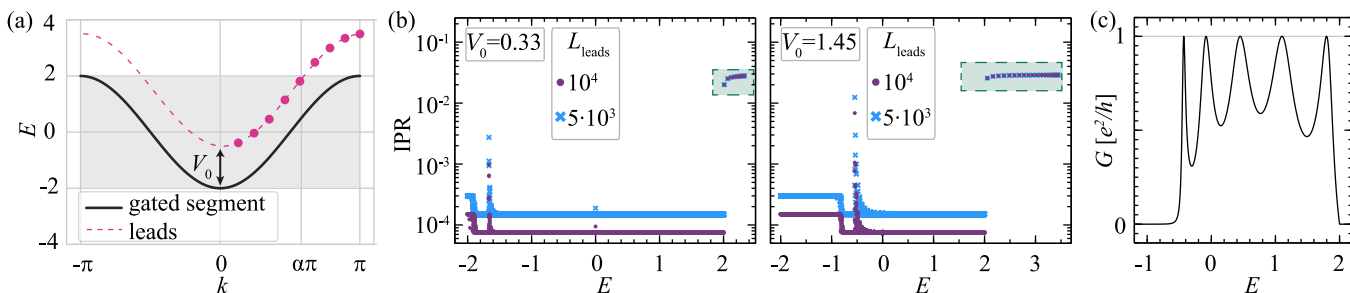


FIG. 2. (a) Dispersion of the infinite leads (black solid line) and of the gated segment in the $L \rightarrow \infty$ limit (pink dashed line). The two dispersions overlap for $k \in [-\alpha\pi, \alpha\pi]$. We also show the energies of an isolated gated segment with $L = 9$ plotted as a function of $q_n = \pi n/L$; $n = 1, 2, \dots, L$ (pink solid dots). Counting the number of discretized energies falling outside of the bandwidth of the leads gives the number of states localized on the gated segment, which in this case is 4 states. (b) IPR for a gated segment of length $L = 50$ with $V_0 = 0.33$ (left) and $V_0 = 1.45$ (right), comparing two different lead sizes, $L_{\text{leads}} = 5 \times 10^3$ and $L_{\text{leads}} = 10^4$. States with $E > 2$ (highlighted by a green rectangle) are localized inside the gated segment and their IPR is independent of the lead size. (c) Conductance through the whole system as a function of energy of the incident particle. Here we used $L = 9$ and $V_0 = 1.45$. We remind that potentials and energies are expressed in units of the hopping amplitude $t = 1$.

$$-e^{\text{arccosh}[V_0/2 - \cos k]} = \frac{\sin[k - k\frac{L+1}{2}]}{\sin[-k\frac{L+1}{2}]}. \quad (3)$$

The task can be conveniently recast into counting the number of $q_n = n\pi/L$ with $n \in \{1, \dots, L\}$ larger than $\alpha\pi \equiv \arccos(\frac{V_0}{2} - 1)$, which is the point in the Brillouin zone where the dispersion of the isolated infinite gated segment intersects the band edge of the isolated leads; see Fig. 2(a). Knowing q_n and α , one can show that the number of states localized on the gated segment is given by

$$N_{\text{loc}} = L - \text{floor}(\alpha L), \quad (4)$$

which is a linearly growing function of L with slope $1 - \alpha$, and it exhibits quasiperiodic fluctuations whenever α is irrational.

We note in passing that the same result can be obtained using Levinson’s theorem [32], appropriately modified for a lattice model, from the phase difference between the states at the bottom and top of the band (see Appendix B).

The quasiperiodicity can be distinctly seen in Fig. 1(b), where we also verify the perfect agreement between the analytical result, Eq. (4), and the numerical calculation of N_{loc} using both the inverse participation ratio (IPR) and transport measurements. Albeit simple, we find this result surprising since the leads and the gated segment are periodic, and there is no additional quasiperiodicity or randomness present in the system.

A. Simple counting argument

It is tempting to interpret the above q_n as the wave vector of a tight-binding chain of length L with open boundary conditions. The argument appears then to be counting the number of discrete eigenenergies of the gated segment, whose dispersion in the limit of infinite length is $E_{\text{gated}}(k) = V_0 - 2 \cos k$, that fall outside the continuous band of the leads, of dispersion $E_{\text{leads}}(k) = -2 \cos k$.

The two dispersions intersect at $k = \pm\alpha\pi$, as illustrated in Fig. 2(a), and one can see that the discrete energies of the gated segment fall outside the band of the leads if $q_n > \alpha\pi$. Recalling that $n = 1, 2, \dots, L$, one can straightforwardly

count such states and obtain $L - \text{floor}(\alpha L)$ for the number of states localized on the gated segment, which coincides with the exact solution, Eq. (4).

This is however only an intuitive, and somewhat incorrect, picture which happens coincidentally to give the correct answer. In the exact calculation, the q_n 's are simply a tool to count the number of solutions and have no direct physical interpretation.

B. Probing localized states

One way to probe the localized states is by computing the IPR of the eigenstates of the Hamiltonian (1),

$$\text{IPR}(E_n) = \frac{\sum_j |\psi_j(E_n)|^4}{\sum_j |\psi_j(E_n)|^2}. \quad (5)$$

The IPR is known to scale as (i) $O(1/L_{\text{tot}})$ for states extended over the whole system of length $L_{\text{tot}} = 2L_{\text{leads}} + L$, where L_{leads} is the number of sites in a single lead; (ii) $O(1/(2L_{\text{leads}}))$ for states localized on the leads (when one allows for a small matrix element due to tunneling across the gated segment); and (iii) $O(1/L)$ for states localized only on the gated segment. We use exact diagonalization and compare the results for two different sizes of leads, 5×10^3 and 10^4 sites, and for different gate potentials. The results for a gated segment with $L = 50$ sites are shown in Fig. 2(b), for $V_0 = 0.33$ and $V_0 = 1.45$ (recall that we work in units where $t = 1$). We see that all the states with energy $E > 2$ have an IPR that is independent of the size of the leads, meaning that these states are localized on the gated segment. The aforementioned states cannot hybridize with the states belonging to the leads as their energy falls outside their bandwidth. On the other hand, states falling within the bandwidth of the leads hybridize and delocalize.

The steplike behavior seen in Fig. 2(b) is a numerical artifact of the diagonalization algorithm. When the energy of the eigenstates is smaller than $-2 + V_0$, the particle cannot propagate across the barrier; however, a small tunneling amplitude exists for finite values of L such that the eigenstates found by diagonalization are even and odd superpositions of the states on the left and on the right lead, and the IPR is approximately $1/(2L_{\text{leads}})$ [which in the figure is indistinguishable from $1/(2L_{\text{leads}} + L)$, the IPR of delocalized states]. As we continue to lower the energy of the eigenstates however, the tunneling amplitude is correspondingly suppressed; when it falls below numerical accuracy, the diagonalization routine is no longer able to find even and odd superpositions of states on the left and on the right lead, but rather sees the left and right lead states as eigenstates of the system. This results in an $\text{IPR} \sim 1/L_{\text{leads}}$ and in the step increase observed when we consider the lowest energy eigenstates.

Another way to directly probe the aforementioned localized states is via energy-dependent transport, i.e., via the conductance

$$G(E) = \frac{e^2}{h} \mathcal{T}(E) \mathcal{T}^*(E), \quad (6)$$

where e is the charge of the particle, E is its incident energy, and \mathcal{T} is the transmission coefficient. The above conductance is observed to have an oscillatory behavior in energy, with maxima reaching the value e^2/h , and the distance be-

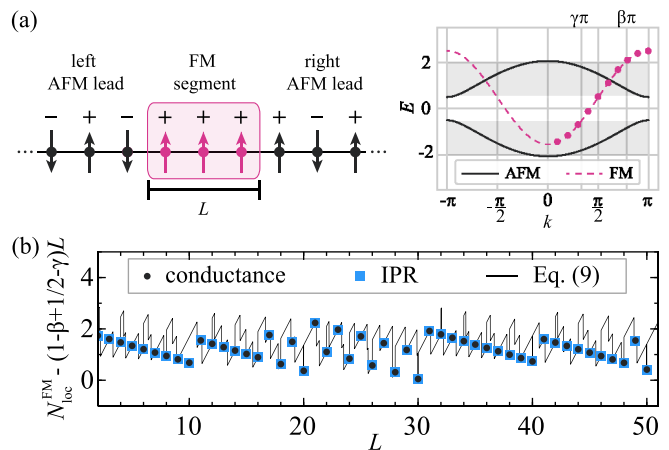


FIG. 3. (a) Left: Illustration of the FM segment in an AFM chain. Black points and arrows illustrate the infinite AFM leads and pink ones illustrate the FM segment of length L , here for $L = 3$. Right: The AFM and FM dispersions for $W = 0.5$. The FM band overlaps with the lower AFM band in the region $k \in [-\gamma\pi, \gamma\pi]$ (for $W \leq 1$) and with the upper AFM band in the region $k \in [-\beta\pi, -\pi/2]$ and $k \in [\pi/2, \beta\pi]$. (b) Number of states localized in the gated region as a function of its length for $W = 0.1$. We subtracted the linear slope $(1 - \beta + 1/2 - \gamma)L$ to emphasize the quasiperiodic nature of the fluctuations following from sampling at integer L . We observe a perfect agreement between numerical data obtained from conductance (black dots), IPR (blue squares), and the analytical prediction in Eq. (9).

tween them determined by the length L (see Appendix D). In Fig. 2(c) we show the numerical result from the simulation of a system consisting of two identical and infinite leads and a gated segment of $L = 9$ sites (see Appendix C for a plot of the conductance as a function of V_0 for fixed L). The peaks in conductance occur once E is in resonance with the energies of the gated segment that hybridize with the leads, i.e., the energies that lie within the bandwidth of the leads. By counting the number of peaks N_{peaks} , whose maxima reach the value e^2/h , we can extract the number of states that localize on the gated segment as $N_{\text{loc}} = L - N_{\text{peaks}}$. The result for the gated chain discussed before is shown in Fig. 1(b). We observe perfect agreement with N_{loc} obtained by IPR, as well as with the analytical prediction (4). Interestingly, a simple analytical calculation of conductance which assumes that the leads do not affect the dispersion of the gated segment gives the same expression for N_{loc} as in Eq. (4); see Appendix D.

III. FERROMAGNETIC SEGMENT IN AN ANTIFERROMAGNETIC CHAIN

Similar quasiperiodic behavior occurs also in related systems of relevance to other experimental settings. Consider for instance the case of an Ising chain where $+$ and $-$ correspond to an on-site energy $\pm W$ for a tight-binding particle along the same chain, with hopping amplitude $t = 1$ (where without loss of generality we set $W > 0$). Specifically, take an infinite antiferromagnetic (AFM) chain with a ferromagnetic (FM) insertion $+\dots+$ of length L [see Fig. 3(a) for a precise illustration of how we define the inserted FM segment].

The dispersion of the AFM leads is given by

$$E_{\text{AFM}}(k) = \pm\sqrt{W^2 + 2(1 + \cos k)}, \quad (7)$$

which exhibits a gap near zero energy, in contrast with the case considered earlier. The dispersion of the FM segment is instead given by the usual relation

$$E_{\text{FM}}(k) = W - 2 \cos k. \quad (8)$$

Both dispersions are illustrated in Fig. 3(a). Note that the FM segment overlaps with both bands of the leads for $W \leq 1$ and only with the upper band for $W > 1$. The FM band overlaps with the lower AFM band for $k \in [-\gamma\pi, \gamma\pi]$ (for $W \leq 1$), where $\gamma\pi \equiv \arccos(W)$, and with the upper AFM band for $k \in \{[-\beta\pi, \pi/2], [\pi/2, \beta\pi]\}$ with $\beta\pi \equiv \arccos[\frac{1}{2}(W - \sqrt{W^2 + 4})]$ [the values of β and γ are visually represented in the right panel of Fig. 3(a) for added clarity].

All states falling outside of the AFM bands correspond to states localized on the FM domain, falling off exponentially when moving into the AFM leads (see Appendix F for examples of wave function profiles). Using a corresponding ansatz for the lattice wave function, as we did for the gated segment earlier, one can explicitly find the localized eigenstates of the system (see Appendix E) by solving equations similar to Eqs. (2) and (3). As shown in Appendix E, the number of states localized on the FM segment with energies above the upper AFM band can be found by counting the number of $q_n = n\pi/L$ with $n \in \{1, \dots, L\}$ larger than $\beta\pi$, i.e., $L - \text{floor}(\beta L)$. Similarly, the number of states localized on the FM segment with energies in the gap of the AFM dispersion can be found by finding the number of $q_n^\infty = n\pi/(L+2) < \pi/2$ and if $W \leq 1$ then subtracting the number of $q_n = n\pi/L \geq \gamma\pi$. This leads to $\text{ceil}(L/2) - \text{floor}(\gamma L)$ localized states in the gap for $W \leq 1$ and $\text{ceil}(L/2)$ for $W > 1$. The total number of states localized on the FM domain is thus given by (Appendix E) [33]

$$N_{\text{loc}}^{\text{FM}} = \begin{cases} L - \text{floor}(\beta L) + \text{ceil}(L/2) - \text{floor}(\gamma L), & W \leq 1, \\ L - \text{floor}(\beta L) + \text{ceil}(L/2), & W > 1. \end{cases} \quad (9)$$

To confirm the above formula, we numerically extract the number of states localized on the FM domain, $N_{\text{loc}}^{\text{FM}}$, using both IPR and conductance. The results for $N_{\text{loc}}^{\text{FM}}$ as a function of size of the FM domain L are shown in Fig. 3(b), where we observe perfect agreement with the analytical prediction, Eq. (9).

As an aside, we note that it is possible to numerically compute the number of localized states on the FM domain more efficiently by counting the number of sign changes in the Sturm sequence obtained by relating the subdeterminants of the Hamiltonian [34]. This enables one to treat larger system sizes at a relatively low computational cost compared to full diagonalization.

IV. CONCLUSIONS

In this paper, we demonstrated how quasiperiodic behavior can emerge in clean periodic systems without driving, borne out of a mechanism similar to the one that gives rise to Wannier-Stark localization [35–37]. For instance, we showed that the number of localized states on a gated segment of a

tight-binding chain (equivalently, the number of peaks in the conductivity along the chain) is a quasiperiodic function of the length of the segment. A similar behavior arises when the tight-binding particle is instead subject to on-site coupling to static Ising degrees of freedom, which form an antiferromagnetic chain with a ferromagnetic segment of finite length inserted into it. We provide both an exact solution as well as an intuitive effective description of the phenomenon, and we discuss how it is directly relevant to various settings, from gated quantum dot arrays to systems described by the Falicov-Kimball model. Similar behavior can be expected in general if a finite segment is inserted into spatially translationally invariant leads. Quasiperiodicity should arise when the dispersion of the inserted segment intersects the band edge of the leads at some $k = \alpha\pi$, with α irrational.

(We note in passing that when both gating and coupling to an underlying spin pattern are present, additional features may appear in the form of states localized at the boundaries of the segment.)

The mechanism discussed in our work is not inherently limited to 1D noninteracting systems and the experimental platforms mentioned in the introduction. Similar mechanisms are expected to operate for example in strongly interacting systems, e.g., quantum wires described by Luttinger liquid theory, that are coupled to leads of finite bandwidth [38–41]. They should also be relevant to two- and higher-dimensional gated systems. One can trivially see it if one uses a separable potential: $V(x, y) = V_0[\Theta(x) + \Theta(y)]$, where Θ is a function that takes the value 1 on a segment of length L and vanishes elsewhere in the system. This potential results in an infinite cross pattern in 2D (of potential V_0), with a raised square at its core (of potential $2V_0$ and size $L \times L$). The exact analytical solution follows directly from the 1D case, and we verified numerically that the agreement is excellent already for L and L_{leads} of the order of a few tens of sites. The case of a simple square potential, where $V = V_0$ only on a region of size $L \times L$ and $V = 0$ elsewhere, is less straightforward and attempting an analytical solution is beyond the scope of the present work. However, one would expect—and indeed numerical simulations suggest—that the quasiperiodic behavior of the number of localized states survives in that case too; the numerical results are unfortunately too limited in accessible system sizes to be conclusive on their own.

On a more speculative note, one may wonder what happens when several FM insertions of different lengths are present in the AFM Ising chain that determines the on-site potential in the Falicov-Kimball-inspired model presented in the main text. Based on our results, one would expect the system to exhibit a quasiperiodically distributed number of quasilocated states that weakly interact with one another via the exponentially decaying tails of their wave functions. The effects of such states on transport as well as on the many-body properties of the system are interesting directions for future work.

ACKNOWLEDGMENTS

We would like to thank O. F. Syljuåsen and A. Szabó for helpful discussions, and J. Chalker for suggesting the connection with Levinson's theorem. C.G. was supported

by the Aker Scholarship. A.Š. acknowledges financial support from the Swiss National Science Foundation (Grant No. 199969). This work was supported in part by the Engineering and Physical Sciences Research Council (EPSRC), Grants No. EP/P034616/1, No. EP/T028580/1, and No. EP/V062654/1.

APPENDIX A: ANALYTICAL DERIVATION OF N_{loc} (DIRECT CALCULATION)

We study an infinite tight-binding chain with constant hopping amplitude $t = 1$ and on-site potential

$$V_n = \begin{cases} 0, & n \leq 0, \\ V_0, & 1 \leq n \leq L, \\ 0, & n \geq L + 1, \end{cases} \quad (\text{A1})$$

where n labels the sites and goes from $-\infty$ to ∞ .

By solving the Schrödinger equation analytically, we derive an expression for the number of states localized on the gated segment. There are two bulk equations, one for the leads and one for the gated segment, given by

$$-\psi_{n-1} - \psi_{n+1} = E\psi_n, \quad (\text{A2})$$

$$-\psi_{n-1} + V_0\psi_n - \psi_{n+1} = E\psi_n. \quad (\text{A3})$$

Using the ansatz $\psi_n = Ae^{ikn}$ separately for the leads and the gated segment, we obtain the dispersions

$$\begin{aligned} E_{\text{gated}}(k) &= V_0 - 2 \cos k, \\ E_{\text{leads}}(k) &= -2 \cos k. \end{aligned} \quad (\text{A4})$$

Being interested in studying the states which localize on the gated segment and decay exponentially into the leads, we construct the following ansatz,

$$\psi_n = \begin{cases} A e^{-(p+i\pi)(L+1)/2} e^{(p+i\pi)n}, & n \leq 0, \\ B \frac{\cos}{\sin} [kn - k(L+1)/2], & 1 \leq n \leq L, \\ \pm A e^{(p+i\pi)(L+1)/2} e^{-(p+i\pi)n}, & n \geq L + 1, \end{cases} \quad (\text{A5})$$

where we have taken advantage of the fact that the potential is symmetric about the middle of the gated region, meaning that the eigenstates must be symmetric or antisymmetric about $(L+1)/2$. Note that $(L+1)/2$ is not restricted to integer values and the following derivation therefore holds irrespective of L being even or odd. Note also that there are only *two possible choices* for the oscillatory phase φ of the wave function in the leads that give real energies: 0 and π . In our case, all the possible localized states are captured by $\varphi = \pi$ and we will thus only consider this case here ($\varphi = 0$ would only give $E < -2$). Having explicitly accounted for the oscillating part of the wave function in the leads, we consider only real $p > 0$. The state in Eq. (A5) has two unknowns: k and the relation between A and B (p is given by requiring $E_{\text{leads}}(p) = 2 \cosh p = E_{\text{gated}}(k)$; namely, $p(k) = \text{arccosh}[V_0/2 - \cos k]$). To find these unknowns, we have to impose the boundary equations which couple the leads and the gated segment. These are in general four equations (two equations for each boundary), but since we have already imposed the exchange symmetry of the wave function, we only need to consider

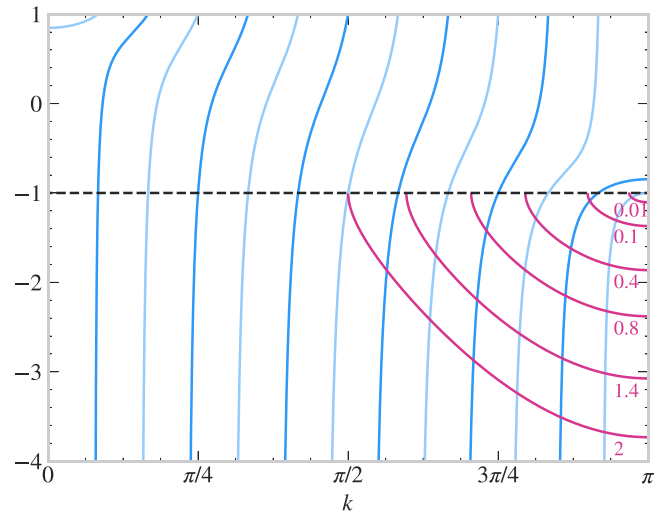


FIG. 4. The pink lines illustrate $LHS(k)$ for different V_0 . The blue lines represent $RHS(k)$ for $L = 12$. The black dashed line shows $C(k) = -1$. The blue lines (RHS) cross this line for $q_n = \pi/Ln$. The pink lines touch $C(k)$ for $\alpha\pi$.

the equations for one of the boundaries. The boundary equations for the left boundary read

$$-\psi_{-1} - \psi_1 = E\psi_0, \quad (\text{A6})$$

$$-\psi_0 + V_0\psi_1 - \psi_2 = E\psi_1. \quad (\text{A7})$$

Inserting the ansatz Eq. (A5) into Eqs. (A6) and (A7), we arrive at the following equation for k :

$$-e^{p(k)} = \frac{\cos \left[k - k \frac{L+1}{2} \right]}{\frac{\cos}{\sin} \left[-k \frac{L+1}{2} \right]}, \quad (\text{A8})$$

with $p(k) = \text{arccosh}[V_0/2 - \cos k]$.

This equation in general has several discrete solutions k_i , and each k_i corresponds to a state localized on the gated segment as long as $p(k_i) > 0$. Finding an explicit expression for the solutions k_i is difficult, but we can count the number of solutions by considering the behavior of the functions on the two sides of the equation.

The left-hand side

$$LHS(k) = -e^{\text{arccosh}[V_0/2 - \cos k]} \quad (\text{A9})$$

is a function starting at $LHS(k) = -1$, for $k = \arccos(V_0/2 - 1) \equiv \alpha\pi$, and decreasing monotonically as $k \rightarrow \pi$; see Fig. 4. For convenience, we define the starting point of LHS as a constant function

$$C(k) = -1. \quad (\text{A10})$$

The right-hand side (of which we have one for the symmetric eigenstates and another for the antisymmetric eigenstates)

$$RHS(k) = \frac{\cos \left[k - k \frac{L+1}{2} \right]}{\frac{\cos}{\sin} \left[-k \frac{L+1}{2} \right]} \quad (\text{A11})$$

is a function with derivative $RHS'(k) \geq 0$ for $k \geq 0$ [and $RHS'(k) = 0$ only for $k = 0, \pi$].

The functions $LHS(k)$ and $RHS(k)$ are illustrated in Fig. 4, where we plot $RHS(k)$, which is independent of V_0 , for $L = 12$, together with $LHS(k)$ for a range of different values of V_0 .

To find an analytical expression for the number of solutions k_i for an arbitrary length L of the gated segment, let us start from the limit $V_0 = 0$ and increase V_0 continuously to see how the number of solutions increases. For $V_0 = 0$ there are no solutions [$\alpha = 1$ and $k = \pi = \alpha\pi$ solves the equation, but this solution is delocalized as $p(\alpha\pi) = 0$ with $E_{\text{gated}}(\alpha\pi) = 2$]. As one then lets $V_0 > 0$, one immediately finds an allowed solution for the RHS line crossing $C(k)$ at π , but for a k_i slightly smaller than π (k_i decreases continuously from π as V_0 increases, approaching the divergence of the corresponding RHS line; see Fig. 4). We then have only one solution until V_0 has increased enough for the next RHS line to fulfill

$$C(\alpha\pi) = RHS(\alpha\pi). \quad (\text{A12})$$

In fact we first get a new allowed solution when V_0 is infinitesimally larger than the value solving Eq. (A12), as $k = \alpha\pi$ gives $p(\alpha\pi) = 0$. Then, upon further increasing V_0 , the number of solutions stays constant (but the values of k_i change continuously) until V_0 is larger than the next value solving Eq. (A12). Consequently, the number of solutions of Eq. (A8) is the number of solutions $C(q) = RHS(q)$ with $q > \alpha\pi$. This follows from the fact that the derivative of RHS is positive, as illustrated in Fig. 4. Here, we see that once an RHS line crosses -1 for $q > \alpha\pi$, it must necessarily also cross LHS(k) for some $k = k_i$ smaller than q and it must give us an allowed solution for this k_i .

It can easily be shown that $C(q) = RHS(q)$ for $q_n = \pi n/L$ with $n \in \{-L, \dots, -1, 1, \dots, L\}$. Counting the number of solutions now reduces to counting how many $q_n = \pi n/L > \alpha\pi$. This set of q 's is indeed not the values k_i solving Eq. (A8), and thus not the proper k 's characterizing the localized eigenstates on the gated segment; they are simply the values which solve $C(q) = RHS(q)$. No physical significance should be given to these q 's other than them being a tool to count the number of solutions of Eq. (A8). Negative k gives the same physical state as positive k and Eq. (A8) is symmetric for $k \rightarrow -k$; thus we only need to count the positive solutions. In summary, we arrive at the condition for solutions of the Schrödinger equation localized on the gated segment

$$n > \alpha L. \quad (\text{A13})$$

As $0 < n \leq L$, the number of such solutions is given by

$$N_{\text{loc}} = L - \text{floor}(\alpha L). \quad (\text{A14})$$

APPENDIX B: ANALYTICAL DERIVATION OF N_{loc} (LEVINSON'S THEOREM)

Levinson's theorem relates the difference in the phase shift of the extended states at zero and infinite momentum to the number of bound states. We here show that Levinson's theorem, appropriately modified for our lattice model, can be used to obtain the number of localized states, and it reproduces our earlier result, Eq. (4). To show this, let us consider the same model as in Appendix A, with finite size for convenience, and focus on the states that are extended on the leads. We write

one ansatz for the antisymmetric states (ψ^A) and one for the symmetric states (ψ^S):

$$\psi_n^A = \begin{cases} A \sin [kn - k \frac{L+1}{2} + \delta^A(k)], & -L_{\text{leads}} < n \leq 0, \\ B \sin [k'n - k' \frac{L+1}{2}], & 1 \leq n \leq L, \end{cases} \quad (\text{B1})$$

$$\psi_n^S = \begin{cases} A \cos [kn - k \frac{L+1}{2} + \delta^S(k)], & -L_{\text{leads}} < n \leq 0, \\ B \cos [k'n - k' \frac{L+1}{2}], & 1 \leq n \leq L, \end{cases} \quad (\text{B2})$$

where the form of the wave function on the right lead follows by symmetry. $\delta^{A(S)}(k)$ is the scattering phase shift defined so that it vanishes for $V_0 = 0$. k' is given by $k' = \arccos(V_0/2 + \cos k)$ and is imaginary for $-2 \leq E < -2 + V_0$ and real for $-2 + V_0 \leq E \leq 2$.

The open boundary conditions of the chain are imposed by assuming $\psi(-L_{\text{leads}}) = \psi(L_{\text{leads}}) = 0$. Consequently, the allowed values of k are those where either of the functions

$$f^A(k) = \left(-kL_{\text{leads}} - k \frac{L+1}{2} + \delta^A(k) \right) / \pi, \quad (\text{B3})$$

$$f^S(k) = \left(-kL_{\text{leads}} - k \frac{L+1}{2} + \delta^S(k) \right) / \pi - \frac{1}{2} \quad (\text{B4})$$

take an integer value.

For sufficiently large L_{leads} , $f^{A(S)}(k)$ is a monotonically decreasing function of k [we require $\frac{\partial \delta}{\partial k} < L_{\text{leads}} + \frac{L+1}{2}$, which includes the requirement that $\delta(k)$ is continuous]. If we consider $f^{A(S)}(k)$ at the minimum and maximum momentum, i.e., $k = 0$ and $k = \pi$, we can then count the number of antisymmetric (symmetric) extended states as

$$N_{\text{ext}}^{A(S)} = \text{ceil}[f^{A(S)}(k=0)] - \text{floor}[f^{A(S)}(k=\pi)] - 1. \quad (\text{B5})$$

We have here paid extra caution to states with momenta $k = 0$ and $k = \pi$, as necessary. Their wave functions are zero everywhere and should thus not be included in the counting. This explains the choices of ceil and floor and why we subtract one in $N_{\text{ext}}^{A(S)}$.

By imposing the boundary equations between the leads and the gated segment, we find that the phase shift is given by

$$\cot \left[\delta^A(k) - k \frac{L+1}{2} \right] = \frac{\sin[k' - k'(L+1)/2]}{\sin[-k'(L+1)/2] \sin k} - \cot k, \quad (\text{B6})$$

$$\tan \left[\delta^S(k) - k \frac{L+1}{2} \right] = -\frac{\cos[k' - k'(L+1)/2]}{\cos[-k'(L+1)/2] \sin k} + \cot k, \quad (\text{B7})$$

where an appropriate integer number of π should be added to the phase shift so that it is continuous.

For $V_0 = 0$, the phase shift is necessarily zero and all states are extended. We then have

$$N_{\text{ext}}^A \big|_{V_0=0} = L_{\text{leads}} - 1 + \text{ceil}[(L+1)/2],$$

$$N_{\text{ext}}^S \big|_{V_0=0} = L_{\text{leads}} + \text{ceil}[L/2],$$

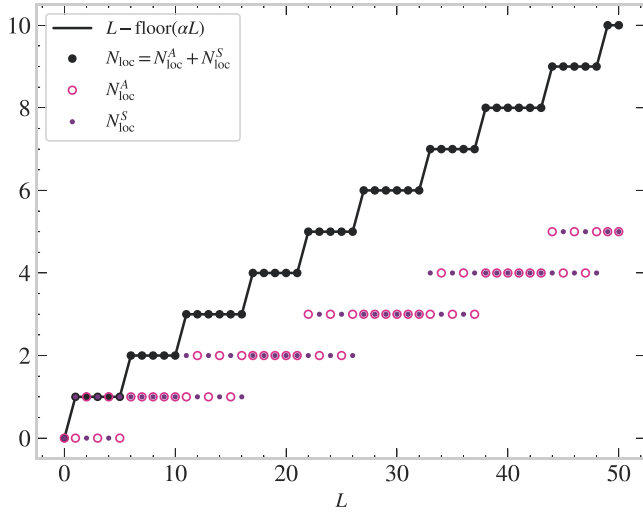


FIG. 5. The number of localized states found from Levinson's theorem compared to $L - \text{floor}(\alpha L)$ for $V_0 = 0.33$.

giving $2L_{\text{leads}} + L$ states in total. As the total number of anti-symmetric and symmetric states both should be independent of V_0 , we find that the number of localized states is

$$N_{\text{loc}}^A = \begin{cases} \frac{1}{\pi} [\delta^A(k = \pi) - \delta^A(k = 0)] + \frac{1}{2}, & L \text{ even,} \\ \frac{1}{\pi} [\delta^A(k = \pi) - \delta^A(k = 0)], & L \text{ odd,} \end{cases} \quad (\text{B8})$$

$$N_{\text{loc}}^S = \begin{cases} \frac{1}{\pi} [\delta^S(k = \pi) - \delta^S(k = 0)] + \frac{1}{2}, & L \text{ even,} \\ \frac{1}{\pi} [\delta^S(k = \pi) - \delta^S(k = 0)] + 1, & L \text{ odd.} \end{cases} \quad (\text{B9})$$

The total number of localized states is $N_{\text{loc}} = N_{\text{loc}}^A + N_{\text{loc}}^S$. Numerically solving for $\delta(k)$, we end up with the number of localized states shown in Figs. 5 and 6, which is in perfect agreement with Eq. (4).

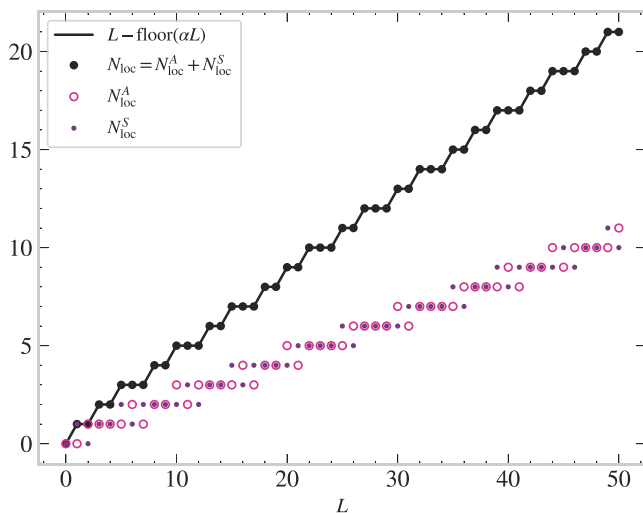


FIG. 6. The number of localized states found from Levinson's theorem compared to $L - \text{floor}(\alpha L)$ for $V_0 = 1.45$.

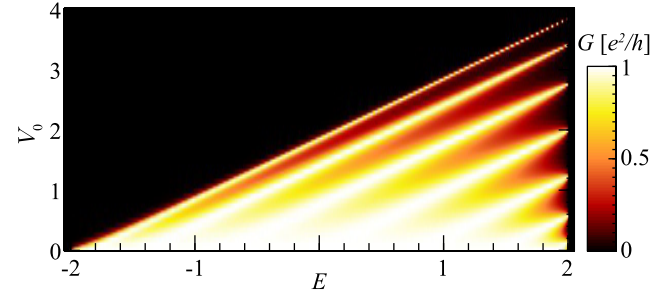


FIG. 7. Conductance as a function of V_0 for $L = 10$, in the gated chain model in Sec. II.

APPENDIX C: DEPENDENCE ON V_0

Figure 7 shows the dependence of peaks in the conductance, from which the number of localized states can be extracted, on V_0 . Notice that the behavior of the system depends continuously on the gated voltage, and $N_{\text{loc}}(V_0)$ does not show quasiperiodic behavior as a function of the gate voltage V_0 .

APPENDIX D: ANALYTICAL CALCULATION OF THE CONDUCTANCE

The conductance through a single-channel 1D system is given by the Landauer formula

$$G(E) = \frac{e^2}{h} \mathcal{T}(E) \mathcal{T}^*(E), \quad (\text{D1})$$

where E is the energy of the incident particle and \mathcal{T} is the transmission coefficient through the gated region. To obtain the transmission coefficient, we first write the wave function of the free particle in continuum in the left and right leads (L, R) and in the gated region (M)

$$\psi_L(x) = e^{ikx} + \mathcal{R}e^{-ikx}, \quad (\text{D2})$$

$$\psi_M(x) = Ae^{ik'x} + Be^{-ik'x}, \quad (\text{D3})$$

$$\psi_R(x) = \mathcal{T}e^{ikx}, \quad (\text{D4})$$

where k and k' are the momenta of the leads and the middle region, respectively. Using the following boundary conditions,

$$\begin{aligned} \psi_L(0) &= \psi_M(0), & \psi_M(L) &= \psi_R(L), \\ \partial_x \psi_L(0) &= \partial_x \psi_M(0), & \partial_x \psi_M(L) &= \partial_x \psi_R(L), \end{aligned} \quad (\text{D5})$$

we obtain the expression for the transmission coefficient

$$\mathcal{T} = \left[1 - \left(\frac{1 + \kappa}{1 - \kappa} \right)^2 \right] \frac{e^{-ikL}}{e^{ik'L} - \left(\frac{1 + \kappa}{1 - \kappa} \right)^2 e^{-ik'L}}, \quad (\text{D6})$$

where $\kappa \equiv k/k'$. The energy dependence is obtained by inverting Eqs. (A4), which gives

$$\begin{aligned} k(E) &= \arccos\left(-\frac{E}{2}\right), \\ k'(E) &= \arccos\left(\frac{V_0 - E}{2}\right), \\ \kappa(E) &= \frac{\arccos\left(-\frac{E}{2}\right)}{\arccos\left(\frac{V_0 - E}{2}\right)}. \end{aligned} \quad (\text{D7})$$

The energy-dependent conductance then follows,

$$G(E) = \frac{\frac{e^2}{h} \left[1 - \left(\frac{1+\kappa}{1-\kappa}\right)^2\right]^2}{1 + \left(\frac{1+\kappa}{1-\kappa}\right)^4 - 2\left(\frac{1+\kappa}{1-\kappa}\right)^2 \cos\left[2 \arccos\left(\frac{V_0 - E}{2}\right)L\right]}. \quad (\text{D8})$$

Note that $G(E)$ is an oscillatory function with maxima reaching $\frac{e^2}{h}$ located at energies E_n that maximize the cosine term in the denominator, namely when

$$\arccos\left(\frac{V_0 - E_n}{2}\right) = \pi \frac{n}{L}, \quad (\text{D9})$$

with $n \in \mathbb{N}$. To count the total number of oscillations in the conductance for a given length L , we first need to restrict the energies E_n to an interval $[-2, 2]$, which is the bandwidth of the leads. The number of oscillations in conductance for a fixed length L is

$$N_{\text{peaks}}(L) = \left\lfloor \frac{L}{\pi} \arccos\left(\frac{V_0}{2} - 1\right) \right\rfloor \quad (\text{D10})$$

$$= \text{floor}(\alpha L), \quad (\text{D11})$$

with the same definition of α as in the main text and in Appendix A.

APPENDIX E: ANALYTICAL DERIVATION OF $N_{\text{loc}}^{\text{FM}}$

The second example we consider in the main text is an infinite tight-binding chain with constant hopping amplitude $t = 1$ and on-site potential

$$V_i = \begin{cases} (-1)^{i+1}W, & i \leq 0, \\ +W, & 1 \leq i \leq L, \\ (-1)^{i+L+1}W, & i \geq L+1, \end{cases} \quad (\text{E1})$$

where i labels the sites and goes from $-\infty$ to ∞ . This can be viewed as a hopping particle interacting with classical Ising spins living on the sites of the chain, arranged in an infinite antiferromagnetic (AFM) pattern with a ferromagnetic (FM) insertion of length L . [Notice that, for convenience, we adopted a labeling convention for the potential in Eq. (E1) such that $L = 0$ corresponds to an infinite AFM pattern.]

We analytically derive the expression for the number of states localized on the FM segment by solving the Schrödinger equation. In this case, the potential is symmetric about $i = (L+2)/2$. Thus, we only need to solve for $i \leq (L+2)/2$ and enforce a symmetric/antisymmetric wave function. Note that $(L+2)/2$ is not restricted to integer values and the following derivation therefore holds irrespective of L being even or odd.

The AFM leads are divided into two sublattices. We therefore have three bulk equations: two for the leads and one for the FM segment, given by

$$-\psi_{n-1}^- + (+W)\psi_n^+ - \psi_n^- = E\psi_n^+, \quad (\text{E2})$$

$$-\psi_n^+ + (-W)\psi_n^- - \psi_{n+1}^+ = E\psi_n^-, \quad (\text{E3})$$

$$-\psi_{n-1}^{\text{FM}} + (+W)\psi_n^{\text{FM}} - \psi_{n+1}^{\text{FM}} = E\psi_n^{\text{FM}}, \quad (\text{E4})$$

where ψ^+ (ψ^-) is the wave function on the sublattice of potential $+W$ ($-W$) in the left AFM lead and ψ^{FM} is the wave function in the FM segment. We have introduced a new index n to label the unit cells, implying $i = 2n - 1, 2n$ in the left lead whereas $i = n$ in the FM segment.

Using the ansatz $\psi_n^+ = Ae^{ikn}$ for the leads, we get the dispersion

$$E_{\text{AFM}}(k) = \pm\sqrt{W^2 + 2(1 + \cos k)}, \quad (\text{E5})$$

and using the ansatz $\psi_n^{\text{FM}} = Ae^{ikn}$ for the FM segment, we get the dispersion

$$E_{\text{FM}}(k) = W - 2\cos k. \quad (\text{E6})$$

We are interested in finding the states which localize on the FM segment and therefore decay exponentially into the leads. To search for such solutions, we construct the following ansatz,

$$\psi_n^+ = Ae^{-(p+i\varphi)(L+2)/2} e^{(p+i\varphi)n}, \quad n \leq 0, \quad (\text{E7})$$

$$\psi_n^{\text{FM}} = B \frac{\cos\left[kn - k\frac{L+2}{2}\right]}{\sin\left[kn - k\frac{L+2}{2}\right]}, \quad 1 \leq n \leq L+1, \quad (\text{E8})$$

where the wave function on the right lead ($n > L$) follows from symmetry considerations.

Inserting the ansatz into the bulk equations, we get

$$E_{\text{AFM}}(p, \varphi) = \pm\sqrt{W^2 + 2[1 + \cosh(p + i\varphi)]} \quad (\text{E9})$$

and

$$\psi_n^- = -\frac{(1 + e^{p+i\varphi})}{E_{\text{AFM}}(p, \varphi) + W} \psi_n^+. \quad (\text{E10})$$

To find the allowed values for k in Eq. (E8), we need to impose the boundary equations which couple the leads and the FM segment (p is given by requiring $E_{\text{AFM}}(p, \varphi) = E_{\text{FM}}(k)$; namely, $p(k) = \text{arccosh}[2\cos^2 k - 2W\cos k - 1]$). The boundary equations for the left boundary read

$$\begin{aligned} -\psi_0^+ - W\psi_0^- - \psi_1^{\text{FM}} &= E\psi_0^-, \\ -\psi_0^- + W\psi_1^{\text{FM}} - \psi_2^{\text{FM}} &= E\psi_1^{\text{FM}}. \end{aligned} \quad (\text{E11})$$

Here, k and $-k$ correspond to the same physical state, and we will only consider $k \geq 0$. Note also that there are only *two possible choices for the oscillatory phase* φ of the wave function in the leads that give real energies: 0 and π . Here we need to consider the two cases separately: An oscillatory phase $\varphi = 0$ gives energies above the upper band, while an oscillatory phase $\varphi = \pi$ gives energies in the gap.

Let us first consider the states above the upper band, $\varphi = 0$. Inserting the ansatz, Eqs. (E7) and (E8), into the boundary

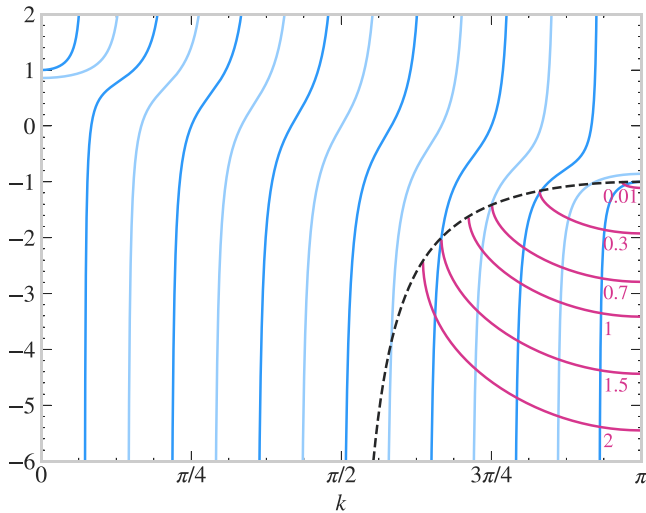


FIG. 8. The pink lines illustrate $LHS^0(k)$ for different values of W . The blue lines represent $RHS(k)$ for $L = 12$. The black dashed line shows $C(k)$. The blue lines (RHS) cross $C(k)$ for $q_n\pi/Ln$. The pink lines (LHS) touch $C(k)$ for $k = \beta\pi$.

equations Eq. (E11), we get the following equation for k :

$$2(\cos k - W) \frac{e^{p(k)}}{1 + e^{p(k)}} = \frac{\cos \left[k - k \frac{L+2}{2} \right]}{\sin \left[-k \frac{L+2}{2} \right]}, \quad (E12)$$

with $p(k) = \text{arccosh}[2 \cos^2 k - 2W \cos k - 1]$. Again, we can quite easily count the number of solutions by considering the behavior of the functions on the two sides of the equation.

The left-hand side

$$LHS^0(k) = 2(\cos k - W) \frac{e^{\text{arccosh}[2 \cos^2 k - 2W \cos k - 1]}}{1 + e^{\text{arccosh}[2 \cos^2 k - 2W \cos k - 1]}} \quad (E13)$$

is a function starting at $LHS^0(k) = \cos k - W$ for $k = \arccos [(-W - \sqrt{W^2 + 4})/2] \equiv \beta\pi$, which decreases monotonically as $k \rightarrow \pi$; see Fig. 8. This is similar to what we had for the gated segment, but now the value of $LHS^0(\beta\pi)$ varies with W . It can be shown that the line $C(k)$ giving the end point of LHS for a certain W is given by

$$C(k) = \frac{1}{\cos k}. \quad (E14)$$

The right-hand side (of which we have one for the symmetric eigenstates and another for the antisymmetric eigenstates)

$$RHS(k) = \frac{\cos \left[k - k \frac{L+2}{2} \right]}{\cos \left[-k \frac{L+2}{2} \right]} \quad (E15)$$

is a function with derivative $RHS'(k) \geq 0$ for $k \geq 0$ [and $RHS'(k) = 0$ only for $k = 0, \pi$].

The functions $LHS^0(k)$ and $RHS(k)$ are plotted in Fig. 8, where we show $RHS(k)$, which is independent of W , for $L = 12$, and $LHS^0(k)$ for a range of different values of W .

To find an analytical expression for the number of solutions k_i of Eq. (E12) for an arbitrary length L of the FM segment, we need to find the solutions of

$$C(q) = RHS(q) \quad (E16)$$

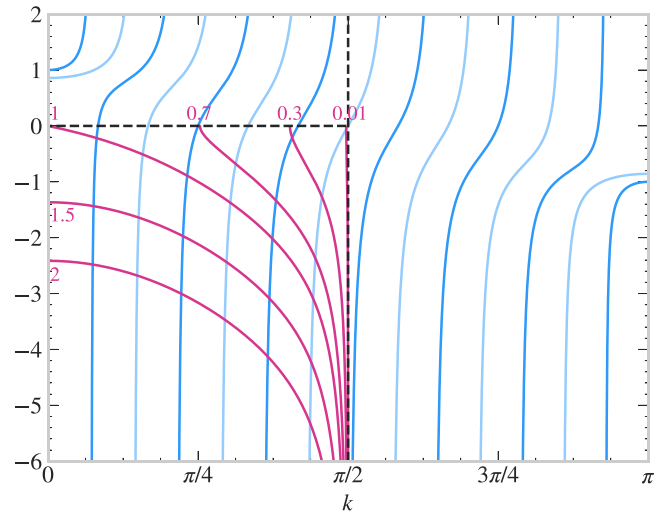


FIG. 9. The pink lines illustrate $LHS^\pi(k)$ for different values of W . The blue lines represent $RHS(k)$ for $L = 12$. The black dashed lines shows $C(k) = 0$ and $k = \pi/2$. The blue lines (RHS) cross $C(k)$ for $q_n = \pi n/Ln$. The pink lines (LHS) touch $C(k)$ for $\gamma\pi$ and diverge to $-\infty$ for $k \rightarrow \pi/2$.

and count the number of solutions q which are larger than $\beta\pi$. It is straightforward to show that $C(q) = RHS(q)$ for $q_n = \pi n/L$ with $n \in \{\text{ceil}(L/2), \dots, L\}$.

Counting the number of solutions now reduces to counting how many $q_n = \pi n/L > \beta\pi$. Note again that we only allow solutions corresponding to real $p(k) > 0$, and $k = \beta\pi$ is thus not an allowed solution. We thus end up with

$$N_{\text{loc}}^0 = L - \text{floor}(\beta L) \quad (E17)$$

states localized on the FM segment with energies above the upper AFM band.

To count the number of localized states with energies in the gap we must set $\varphi = \pi$. $LHS(k)$ then becomes

$$LHS^\pi(k) = -2(\cos k - W) \frac{e^{\text{arccosh}[-2 \cos^2 k + 2W \cos k + 1]}}{1 - e^{\text{arccosh}[-2 \cos^2 k + 2W \cos k + 1]}} \quad (E18)$$

while $RHS(k)$ stays the same as in Eq. (E15). $LHS^\pi(k)$ starts at $k = \gamma\pi \equiv \arccos W$ with $LHS^\pi(\gamma\pi) = 0$ [$k = 0$ for $W > 1$ with $LHS^\pi(0) = -2(1 - W)e^{\text{arccosh}(2W-1)}/(1 - e^{\text{arccosh}(2W-1)})$] and decreases continuously as $k \rightarrow \pi/2$, where it diverges to $-\infty$.

The functions $LHS^\pi(k)$ and $RHS(k)$ are plotted in Fig. 9 for a range of different values of W .

In this case, counting the number of solutions reduces to counting the number of solutions to $RHS(q) = 0$ with $q > \gamma\pi$ which belongs to an RHS line that diverges to $-\infty$ for some $k < \pi/2$. $RHS(q) = 0$ for $q_n = \pi n/L$ with $n \in \{1, \dots, L - 1\}$ and $RHS(q^\infty) \rightarrow -\infty$ for $q_n^\infty = \pi n/(L + 2)$ with $n \in \{1, \dots, L + 1\}$. To find the number of solutions, we subtract the number of $q_n \leq \gamma\pi$ (for $W > 1$, we subtract the number of $q_n < 0$, which is trivially zero) from the number of $q_n^\infty < \pi/2$. Note that $k = \gamma\pi$ and $k = \pi/2$ are not allowed solutions, as these have $p = 0$.

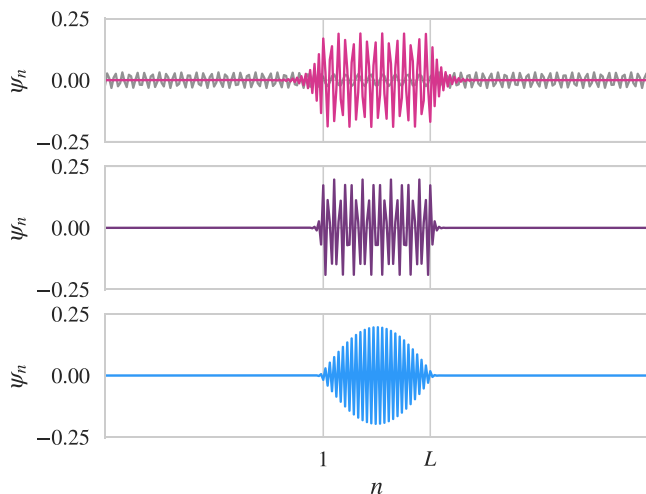


FIG. 10. Examples of eigenstate wave functions localized on the gated segment for $V_0 = 1.45$ and $L = 50$. Top: $E = 2.06$. Middle: $E = 2.95$. Bottom: $E = 3.45$. The top panel also shows a delocalized state with $E = 0.566$ in light gray for comparison.

The total number of $q_n^\infty < \pi/2$ is $\text{ceil}(L/2)$ and the total number of $q_n \leq \gamma\pi$ is $\text{floor}(\gamma L)$. We therefore have

$$N_{\text{loc}}^\pi = \begin{cases} \text{ceil}(L/2) - \text{floor}(\gamma L), & W \leq 1, \\ \text{ceil}(L/2), & W > 1, \end{cases} \quad (\text{E19})$$

states which localize in the gap.

The total number of states localized on the FM segment is thus

$$N_{\text{loc}}^{\text{FM}} = N_{\text{loc}}^0 + N_{\text{loc}}^\pi = \begin{cases} L - \text{floor}(\beta L) + \text{ceil}(L/2) - \text{floor}(\gamma L), & W \leq 1, \\ L - \text{floor}(\beta L) + \text{ceil}(L/2), & W > 1. \end{cases} \quad (\text{E20})$$

APPENDIX F: WAVE FUNCTION PROFILES

We present here some illustrative examples of the eigenstate wave functions localized on the gated/ferromagnetic segment discussed in our work.

Figure 10 shows examples of wave functions with energies $E > 2$ for the gated chain model in Sec. II. The localized behavior is clearly evident for $E > 2$, when compared to a delocalized state for $E < 2$ shown in the top panel for reference (light gray curve).

Figure 11 shows similar examples of eigenstate wave functions for the ferromagnetic segment in an antiferromagnetic chain model in Sec. III.

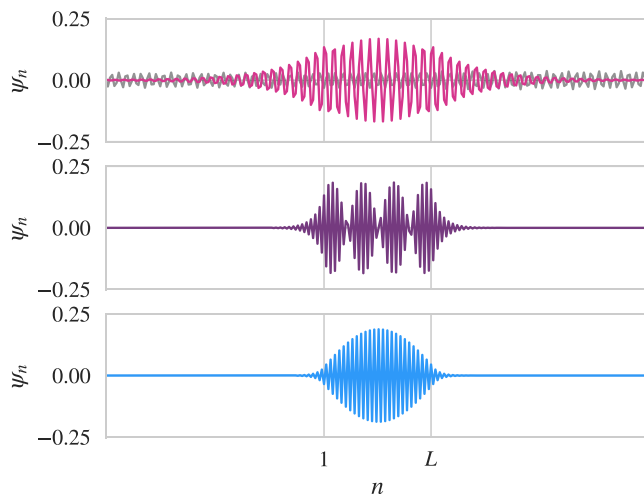


FIG. 11. Examples of eigenstate wave functions localized on the ferromagnetic segment for $W = 0.1$ and $L = 50$. Top: $E = 0.0265$ (in the gap). Middle: $E = 2.05$. Bottom: $E = 2.10$. The top panel also shows a delocalized state with $E = 0.543$ in light gray for comparison.

APPENDIX G: SPECIAL CASES

While the quasiperiodic behavior discussed in the main text is generic, there are fine-tuned values of the system parameters when it disappears. For completeness, we review them here briefly for the two models considered in our work.

1. Gated segment

In the case of the gated segment, N_{loc} shows *periodic* fluctuations about its linear behavior whenever α is rational, implying that $\alpha\pi = \arccos(V_0/2 - 1)$ is a rational number times π . This occurs for an infinite set of fine-tuned values of V_0 (e.g., $V_0 = \{2 - \sqrt{2}, 1, 2\}$); however, it is a set of measure zero on the real line.

2. Ferromagnetic segment in an antiferromagnetic chain

Let us now consider the example of a ferromagnetic segment in an antiferromagnetic chain. For $W \geq 1$, $N_{\text{loc}}^{\text{FM}}$ only depends on β and the situation is very similar to that of the gated segment. If β is rational, which happens for an infinite but sparse number of values W , $N_{\text{loc}}^{\text{FM}}$ shows periodic fluctuations. In the case of $W < 1$, $N_{\text{loc}}^{\text{FM}}$ depends on both β and γ and it only loses its quasiperiodic behavior if both β and γ are rational. We only find one value of W where this happens, namely $W = \sqrt{2}/2$.

- [1] L. D. Landau and E. M. Lifshitz, *Mechanics: Course of Theoretical Physics*, 3rd ed., Vol. 1 (Pergamon Press, 1960).
 [2] T. Shinbrot, C. Grebogi, J. Wisdom, and J. Yorke, Chaos in a double pendulum, *Am. J. Phys.* **60**, 491 (1992).
 [3] Z. F. Ezawa, *Quantum Hall Effects: Recent Theoretical and Experimental Developments*, 3rd ed. (World Scientific Publishing, 2013).

- [4] The reader should bear in mind here, for reference, the concept of Wannier-Stark localization [35–37].
 [5] S. Krinner, D. Stadler, D. Hushman, J. Brantut, and T. Esslinger, Observation of quantized conductance in neutral matter, *Nature (London)* **517**, 64 (2015).
 [6] M. Lebrat, P. Grišins, D. Hushman, S. Häusler, L. Corman, T. Giamarchi, J.-P. Brantut, and T. Esslinger, Band and Correlated

- Insulators of Cold Fermions in a Mesoscopic Lattice, *Phys. Rev. X* **8**, 011053 (2018).
- [7] T. Monz, P. Schindler, J. T. Barreiro, M. Chwalla, D. Nigg, W. A. Coish, M. Harlander, W. Hänsel, M. Hennrich, and R. Blatt, 14-Qubit Entanglement: Creation and Coherence, *Phys. Rev. Lett.* **106**, 130506 (2011).
- [8] N. Friis, O. Marty, C. Maier, C. Hempel, M. Holzäpfel, P. Jurcevic, M. B. Plenio, M. Huber, C. Roos, R. Blatt, and B. Lanyon, Observation of Entangled States of a Fully Controlled 20-Qubit System, *Phys. Rev. X* **8**, 021012 (2018).
- [9] D. M. Zajac, T. M. Hazard, X. Mi, E. Nielsen, and J. R. Petta, Scalable Gate Architecture for a One-Dimensional Array of Semiconductor Spin Qubits, *Phys. Rev. Appl.* **6**, 054013 (2016).
- [10] X.-Y. Guo, Z.-Y. Ge, H. Li, Z. Wang, Y.-R. Zhang, P. Song, Z. Xiang, X. Song, Y. Jin, L. Lu, K. Xu, D. Zheng, and H. Fan, Observation of Bloch oscillations and Wannier-Stark localization on a superconducting quantum processor, *npj Quantum Inf.* **7**, 51 (2021).
- [11] E. Altman, K. R. Brown, G. Carleo, L. D. Carr, E. Demler, C. Chin, B. DeMarco, S. E. Economou, M. A. Eriksson, K.-M. C. Fu, M. Greiner, K. R. Hazzard, R. G. Hulet, A. J. Kollár, B. L. Lev, M. D. Lukin, R. Ma, X. Mi, S. Misra, C. Monroe *et al.*, Quantum simulators: Architectures and opportunities, *PRX Quantum* **2**, 017003 (2021).
- [12] L. M. Falicov and J. C. Kimball, Simple Model for Semiconductor-Metal Transitions: SmB_6 and Transition-Metal Oxides, *Phys. Rev. Lett.* **22**, 997 (1969).
- [13] A. Smith, J. Knolle, D. L. Kovrizhin, and R. Moessner, Disorder-Free Localization, *Phys. Rev. Lett.* **118**, 266601 (2017).
- [14] M. Schreiber, S. S. Hodgman, P. Bordia, H. P. Lüschen, M. H. Fischer, R. Vosk, E. Altman, U. Schneider, and I. Bloch, Observation of many-body localization of interacting fermions in a quasirandom optical lattice, *Science* **349**, 842 (2015).
- [15] P. Bordia, H. Lüschen, S. Scherg, S. Gopalakrishnan, M. Knap, U. Schneider, and I. Bloch, Probing Slow Relaxation and Many-Body Localization in Two-Dimensional Quasiperiodic Systems, *Phys. Rev. X* **7**, 041047 (2017).
- [16] V. K. Varma and M. Žnidarič, Diffusive transport in a quasiperiodic Fibonacci chain: Absence of many-body localization at weak interactions, *Phys. Rev. B* **100**, 085105 (2019).
- [17] N. Macé, N. Laflorencie, and F. Alet, Many-body localization in a quasiperiodic Fibonacci chain, *SciPost Phys.* **6**, 050 (2019).
- [18] D. Johnstone, P. Öhberg, and C. W. Duncan, Mean-field phases of an ultracold gas in a quasicrystalline potential, *Phys. Rev. A* **100**, 053609 (2019).
- [19] R. Ghadimi, T. Sugimoto, and T. Tohyama, Mean-field study of the Bose-Hubbard model in the Penrose lattice, *Phys. Rev. B* **102**, 224201 (2020).
- [20] M. Sbroscia, K. Viebahn, E. Carter, J.-C. Yu, A. Gaunt, and U. Schneider, Observing Localization in a 2D Quasicrystalline Optical Lattice, *Phys. Rev. Lett.* **125**, 200604 (2020).
- [21] F. Flicker, S. H. Simon, and S. A. Parameswaran, Classical Dimers on Penrose Tilings, *Phys. Rev. X* **10**, 011005 (2020).
- [22] A. Szabó and U. Schneider, Mixed spectra and partially extended states in a two-dimensional quasiperiodic model, *Phys. Rev. B* **101**, 014205 (2020).
- [23] A. Štrkalj, E. V. H. Doggen, I. V. Gornyi, and O. Zeitler, Many-body localization in the interpolating Aubry-André-Fibonacci model, *Phys. Rev. Res.* **3**, 033257 (2021).
- [24] M. O. Oktel, Strictly localized states in the octagonal Ammann-Beenker quasicrystal, *Phys. Rev. B* **104**, 014204 (2021).
- [25] F. A. An, K. Padavić, E. J. Meier, S. Hegde, S. Ganeshan, J. H. Pixley, S. Vishveshwara, and B. Gadway, Interactions and Mobility Edges: Observing the Generalized Aubry-André Model, *Phys. Rev. Lett.* **126**, 040603 (2021).
- [26] A. J. Friedman, B. Ware, R. Vasseur, and A. C. Potter, Topological edge modes without symmetry in quasiperiodically driven spin chains, *Phys. Rev. B* **105**, 115117 (2022).
- [27] U. Agrawal, R. Vasseur, and S. Gopalakrishnan, Quasiperiodic many-body localization transition in dimension $d > 1$, *Phys. Rev. B* **106**, 094206 (2022).
- [28] A. Štrkalj, E. V. H. Doggen, and C. Castelnuovo, Coexistence of localization and transport in many-body two-dimensional Aubry-André models, *Phys. Rev. B* **106**, 184209 (2022).
- [29] S. Gopalakrishnan, I. Martin, and E. A. Demler, Quantum Quasicrystals of Spin-Orbit-Coupled Dipolar Bosons, *Phys. Rev. Lett.* **111**, 185304 (2013).
- [30] E. Sagi and Z. Nussinov, Emergent quasicrystals in strongly correlated systems, *Phys. Rev. B* **94**, 035131 (2016).
- [31] F. Mivehvar, H. Ritsch, and F. Piazza, Emergent Quasicrystalline Symmetry in Light-Induced Quantum Phase Transitions, *Phys. Rev. Lett.* **123**, 210604 (2019).
- [32] N. Levinson, On the Uniqueness of the Potential in a Schrödinger Equation for a Given Asymptotic Phase, *Danske Vid. Selsk. Mat.-Fys. Medd.* **25**, 29 (1949).
- [33] A similar simple counting argument can be used here as we did in the case of the gated segment. However, it seems only to be able to reproduce the exact expression in Eq. (9) up to an additive unit constant.
- [34] J. M. Ortega, On Sturm sequences for tridiagonal matrices, *J. ACM* **7**, 260 (1960).
- [35] F. Bloch, Über die Quantenmechanik der Elektronen in Kristallgittern, *Z. Phys.* **52**, 555 (1929).
- [36] C. Zener, A theory of the electrical breakdown of solid dielectrics, *Proc. R. Soc. London A* **145**, 523 (1934).
- [37] G. H. Wannier, Dynamics of band electrons in electric and magnetic fields, *Rev. Mod. Phys.* **34**, 645 (1962).
- [38] I. Safi and H. J. Schulz, Transport in an inhomogeneous interacting one-dimensional system, *Phys. Rev. B* **52**, R17040(R) (1995).
- [39] Y. V. Nazarov, A. A. Odintsov, and D. V. Averin, Tunnel density of states in a Luttinger constriction, *Europhys. Lett.* **37**, 213 (1997).
- [40] D. B. Gutman, Y. Gefen, and A. D. Mirlin, Bosonization of one-dimensional fermions out of equilibrium, *Phys. Rev. B* **81**, 085436 (2010).
- [41] A. Štrkalj, M. S. Ferguson, T. M. R. Wolf, I. Levkivskyi, and O. Zeitler, Tunneling into a Finite Luttinger Liquid Coupled to Noisy Capacitive Leads, *Phys. Rev. Lett.* **122**, 126802 (2019).